water

MDPI

Article

Photocatalytic Degradation of Polyamide 66; Evaluating the Feasibility of Photocatalysis as a Microfibre-Targeting Technology

Jae-Mee Lee [1], Rosa Busquets [1,2], In-Cheol Choi [3], Sung-Ho Lee [4], Jong-Kyu Kim [5,*] and Luiza C. Campos [1,*]

1 Department of Civil, Environmental and Geomatic Engineering, University College London, London WC1E 6BT, UK; jae.lee.19@ucl.ac.uk (J.-M.L.); R.Busquets@kingston.ac.uk (R.B.)
2 Faculty of Science, Engineering and Computing, Kingston University, Surrey KT1 2EE, UK
3 National Institute of Environmental Research/Environment Infrastructure Research, Incheon 22689, Korea; cic00@korea.kr
4 SK Incheon Petrochem, Incheon 22771, Korea; miso1204@sk.com
5 Department of Civil, Urban and Real Estate Development, Shinhan University, Uijeongbu 11644, Korea
* Correspondence: jkim@shinhan.ac.kr (J.-K.K.); l.campos@ucl.ac.uk (L.C.C.); Tel.: +82-(10)-6320-8718 (J.-K.K.); +44-(0)20-7679-4162 (L.C.C.)

Received: 22 November 2020; Accepted: 14 December 2020; Published: 17 December 2020

Abstract: Wastewater treatment plants (WWTPs) have been identified as main contributors to releasing microfibres into the environment, however, WWTPs do not have microfibre-targeting technologies. In this study, photocatalysis is evaluated as a potential technology to treat microfibres in WWTPs by studying the degradation of polyamide 66 (PA66) microfibres using ultraviolet (UV) and titanium dioxide (TiO_2). PA66 microfibres suspended in deionised water were exposed to different combinations of UV and TiO_2. The degradation of the PA66 microfibres was monitored by changes in mass, carbonyl index and morphology using microbalance, infrared spectroscopy, and scanning electron microscopy. The formation of by-products from the degradation of the fibres was evaluated by measuring the chemical oxygen demand (COD) of the treated water. The degradation efficiency was optimised under UVC with a dose of 100 mg TiO_2/L. Under these conditions, the PA66 microfibres presented a 97% mass loss within 48 h. The photocatalytic conditions applied generated a relatively low level of by-products (<10 mg/L of COD). Therefore, photocatalysis with TiO_2 an UVC could potentially be a feasible technology to treat microfibres in WWTPs, although more investigation is required to establish if this treatment leads to the formation of nanofibres. Further work is needed to translate the present optimised conditions to WWTPs.

Keywords: nylon; microfibre; photocatalysis; wastewater; microplastics; titanium dioxide

1. Introduction

The global demand, production, and generation of plastic waste have skyrocketed over the last 60 years [1]. Plastics have penetrated all aspects of our daily life: they are included, among many applications, in clothing, packaging, materials used in construction, and agriculture. Global plastic production and their utilisation has increased from 1.5 to 335 million metric tons from 1950 to 2016 [2]. Plastics present excellent properties of durability that result in resistance to natural degradation. However such high stability is not advantageous considering that globally, from the 1980, plastic wastes have been mainly discarded [1]: more than half of the plastic waste ends up in landfills or in the environment rather than being recycled or incinerated [3]. Due to the immense plastic production and improper waste management, plastic pollution is of great concern [4,5]. Specifically, microfibres

are considered the most significant class of microplastic (MP) pollution in terms of its ubiquity and ecotoxicity [6,7].

MPs are defined as plastic debris with a particle size of 0.001–<5 mm [8], or 0.001–<1 mm [4,9]. They can be categorised into primary and secondary MPs depending on if they enter the environment from the in-use stock in the MP dimensions, or if the particles resulted from the breakdown of the larger plastics for instance by chemical, physical, and biological forces, including UV light, mechanical forces, oxidation, heat, and biodegradation [10]. Moreover, a recent work has found that a freshwater organism can fragment microplastics [11].

Recent research is focusing on whether microbeads, fragments, and microfibres have a detrimental impact to aquatic organisms. The exposure of aquatic biota to MPs may impact on feeding activity [12], growth rate [13], fecundity [14,15], and survival [16]. There is evidence that microplastics can transport various pollutants such as persistent organic pollutants [17]. Moreover, it has been reported that a person can potentially be consuming, on average, 1769 particles of MPs every week just from drinking water [18] and that MPs can accumulate in the human body [19,20]. The potential health risks of MPs for humans are speculated from animal testing showing that MPs can enter tissues and cells. Based on results from animal testing, once the MPs enter the human body through ingestion or inhalation, they can cause inflammatory response in the digestive system [21]. Moreover, since other pollutants (e.g., persistent organic pollutants, metals, and pathogenic microorganisms) or plastic additives can become part of the MPs, the leaching of these pollutants can exacerbate the toxic effects of MPs [22].

Among diverse pathways leading to the entrance of MP contamination in water bodies, wastewater discharged from wastewater treatment plants (WWTPs) has been identified as a main contributor [23]. Some of MPs can be removed through skimming, sedimentation, and filtration in general WWTPs, however none of these processes are originally designed for MPs removal [24–26] Consequently, significant amounts of MPs in WWTPs may escape with the effluent and enter aquatic ecosystems [27–29]. Up to now, to the best of our knowledge, no microfibre-targeted treatment process has been applied in any full-scale WWTPs and membrane technology to separate microfibres from water is still at the preliminary research stage [26]. Therefore, there is need for developing technologies that can treat microfibres in WWTPs.

The most prevalent type of MPs identified in the effluent of wastewater are fibres, with polyamide (PA), polyester (PEST), and polyethylene terephthalate (PET) being common [26,30,31], although the types of microfibres may be affected by the clothing used in every country. In agreement with the release of fibres through wastewater effluents, a recent review by the authors also identified that this is the main MP in freshwater systems [32]. Research on monitoring, detection, and quantification of microfibres is relatively well-established, while studies on treatment or removal methods of microfibres are emerging. The current remediation processes to treat microfibres and other types of MPs include incineration or filtration. However, these methods generate unwanted by-products or require high energy [33]. Thus, advanced oxidation processes (AOPs) have been recognised as a potential technology for degrading plastic wastes because they can remove recalcitrant organics with relatively low formation of by-products [33,34]. Consequently, AOPs, which involve the generation of highly reactive hydroxyl radical (•OH) that can degrade organic contaminants, have been extensively applied to treat pollutants in WWTPs [34–36]. Particularly, AOP using UV irradiation and titanium dioxide (TiO_2) as a catalyst has grown acceptance as a successful technology to treat wastewater [37].

Several laboratory investigations have studied the effect of photocatalytic oxidation of MPs, in particular, of polyethylene (PE) film [35,38–40] and polystyrene (PS) beads [36,41]. The effect of photodegradation of fibres has not been studied to the best of our knowledge. In this research, photo-oxidation and photocatalytic degradation of polyamide 66 (PA66) microfibres—one of the most prevalent types MPs in WWTPs—are evaluated in water using UV irradiation and TiO_2. Since there is no research assessing the degradation of PA66 microfibres using photocatalysis as a microfibres-targeted technology, the present study is the first of this kind.

2. Materials and Methods

To investigate the degradation of PA66 microfibres with photo-oxidative and photocatalytic degradation, the experiments were conducted under customised lab-scale reaction chambers as carried out by several authors [35,40,42]. Two sets of experiments were conducted to find (1) the effect of different UV wavelengths and (2) the effect of the TiO_2 dose on the degradation of PA66 microfibres. The degradation of the microfibres was evaluated by the means of mass loss and morphological and chemical changes in the fibres and in the water being treated. All experiments were carried out in triplicate.

2.1. Materials

Synthetic PA66 microfibres with a diameter of 10 µm (AM325705, Goodfellow, UK) were cut with 1.0 m length (≈1.3 mg) using scissors. Mass loss was measured with an analytical microbalance (Mettler AT201, Columbus, OH, USA) with readability of 0.01 mg. Each of the microfibre samples were rinsed with deionised water, pat dried to remove moisture, and stored in a glass container at a room temperature as demonstrated in Figure 1. For the photocatalyst, TiO_2 powder (Aeroxide P25 Degussa, Sigma Aldrich, St. Louis, MO, USA) was used. The TiO_2 powder contained 70% anatase and 30% of rutile with mean particle size of 21 nm. Two types of UV lamps were used: a UVA lamp (Philips TL8W BLB, Łódź, Poland) that allows working at 365 nm, a UVC lamp (Philips TUV 8W, Łódź, Poland) to work at 254 nm.

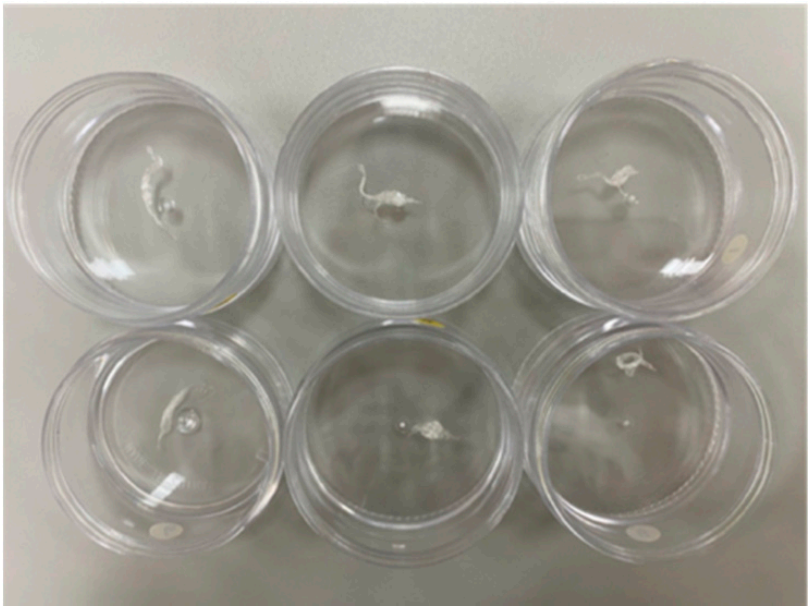

Figure 1. Prepared polymiade 66 (PA66) microfibre samples.

2.2. Construction of Photocatalytic Degradation Reaction Chambers

The reaction chamber used is shown in Figure 2. It was constructed with a glass chamber (length × width × height of 35 × 20 × 25 cm) and it included five UV lamps. The UV lamps and the cover of the chamber were assembled as an integral part to keep the same distance from the UV lamps to the samples and to make it convenient to open and close the chamber when taking out the samples. The distance between the UV lamps and the PA66 microfibre samples was fixed at 5 cm to create homogeneous light intensity. Five electrical stabilisers (8 W) were connected to a single cord to allow turning on and off the UV lamps simultaneously. The chamber was covered with aluminium foil to block stray light and to increase the reflection efficiency. The aluminium cover was perforated (eight openings) for ventilation.

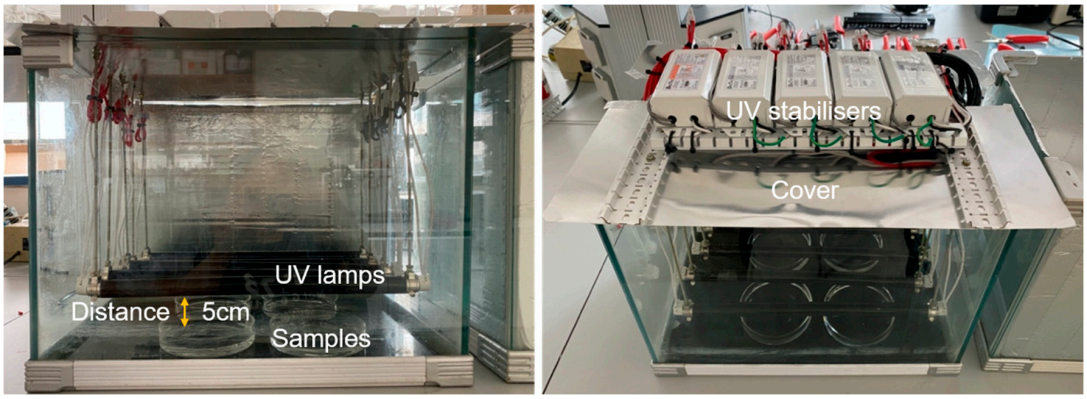

(**a**) (**b**)

Figure 2. Example of one of the three reaction chambers constructed. (**a**) Sideview of the chamber showing the location of the samples, ultraviolet (UV) lamps and distance between the UV lamps and the sample. (**b**) Top-view showing the placement of UV stabilisers and the aluminium cover.

2.3. Experimental Design

The treatment of PA66 microfibres suspended in water by photooxidation and photocatalytic degradation was conducted in the reaction chambers as demonstrated in Figure 3. Three chambers were constructed: one chamber did not include UV lamps; one chamber had five UVC lamps (8 W); and one chamber had five UVA lamps (8 W). The effects of UV light on the fibres was investigated by comparing the impact of short UV wavelengths (UVC), long UV wavelengths (UVA), and no light conditions. Specifically, chamber A was a control (with no lamps) used to monitor fibres hydration and adsorption of TiO_2 onto the fibres. Chamber B was used to investigate the photo-oxidation and photocatalytic oxidation under UVA. Chamber C was equivalent to Chamber B but including UVC instead of UVA. The temperature inside the reaction chamber ranged between 25 and 38 °C under the exposure of UV light without any interruption or control of the temperature. Each sample (dry microfibre) was taken out from the chambers and weighed every 24 h, for up to 105 h reaction time. The final reaction time was selected when reaching >80% fibre mass loss. Then, the changes caused by the degradation were measured in the remaining PA66 microfibres. The PA66 microfibres were returned to the Petri dishes after every mass measurement and repeated this sequence until 105 h of reaction time was reached.

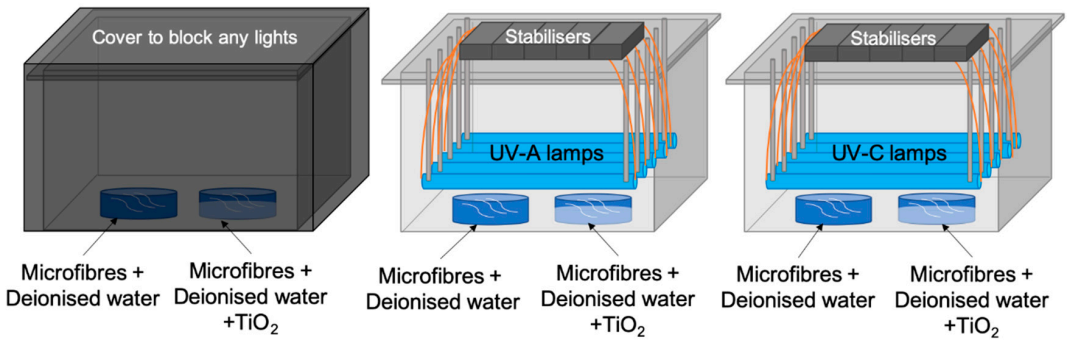

(**a**) (**b**) (**c**)

Figure 3. Illustration of the experimental set-up. The illustration is not shown to scale. Chamber (**a**) is covered to block any light. Chamber (**b**) is equipped with five UVA lamps; chamber (**c**) is equipped with five UVC lamps.

The cut PA66 microfibres (1 m each) were immersed in deionised water (50 mL) in every Petri dish, six Petri dishes were used in total (see Figure 4). The experiments involved 1 m long microfibre

per dish. This set up helped to avoid scattering of microsized fibres. The maximum volume that could be contained in the petri dish was 50 mL of water and this volume made possible the measurement of chemical oxygen demand (COD). Six samples (each sample is a suspension of one fibre in water), labelled as SP1 to SP6 were placed inside of the reaction chambers (A, B, and C). SP2, SP4, and SP6 were mixed with TiO_2 using a magnetic stirrer for 15 min to create a slurry-type condition for the photocatalytic oxidation. No catalyst was added to SP1, SP3, and SP5. The evaporation rate of deionised water due to the applied UV irradiation was evaluated prior to the experiment by measuring the time taken to evaporate 50 mL of deionised water under such experimental conditions. Thus, deionised water was added to the samples every 15 h based on the evaporation rate of 1.25 mL/h to keep the PA66 microfibre samples hydrated and keep the volume in the Petri dish constant. The conditions applied to SP1–SP6 are summarised in Table 1.

(**a**) (**b**) (**c**)

Figure 4. Prepared PA66 microfibre samples immersed in 50 mL of deionised water in Petri dishes placed in each chamber (**a**–**c**). SP1, SP3, and SP5 did not include TiO_2, and SP2, SP4, and SP6 contained 1g of TiO_2 each. SP is refers to sample.

Table 1. Conditions applied to the samples (SP1 to SP6). A triplicate study was carried out for each condition.

	Chamber A		Chamber B		Chamber C	
Samples	SP1	SP2	SP3	SP4	SP5	SP6
Phenomenon	Hydration	Adsorption	Photo-oxidation	Photocatalysis	Photo-oxidation	Photocatalysis
Deionised water (mL)	50	50	50	50	50	50
Distance between the samples and UV lamps (cm)	N/A	N/A	5	5	5	5
TiO_2 (g)	-	1	-	1	-	1
PA66 microfibre (mg)	1.27	1.26	1.29	1.29	1.28	1.27
UV irradiation	N/A		UVA (365 nm)		UVC (254 nm)	
UV lamp power (W)	N/A		40		40	

For the determination of the TiO_2 dose, UV radiation was fixed and a single chamber was used with five samples containing different levels of TiO_2 (Figure 5).

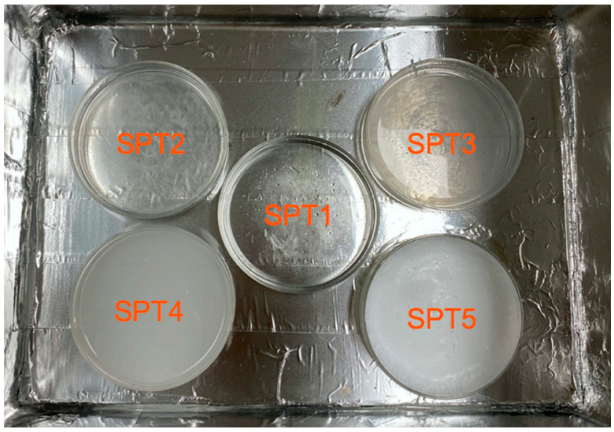

Figure 5. Sample prepared (SPT1 to SPT5) for the optimisation of TiO_2 dose under UVC.

The conditions used for the optimisation of TiO_2 dose are summarised in Table 2. In this second experiment, UVC was used for 48 h. The total reaction time was selected based on a mass loss > 90%. The most effective concentration of TiO_2 was evaluated by means of the fibres' mass loss.

Table 2. Summary of the set-up for SP1-SP5 investigating the optimal concentration of TiO_2 under UVC. Each condition was studied in triplicate.

	SPT1	SPT2	SPT3	SPT4	SPT5
Degradation mechanism			Photocatalysis		
Volume of deionised water (mL)	50	50	50	50	50
TiO_2 (mg)	0	5	25	50	1000
TiO_2 concentration (mg/L)	0	100	500	1000	20,000
Microfibre (mg)	1.21	1.25	1.27	1.25	1.21
UV irradiation	UVC	UVC	UVC	UVC	UVC
UV lamp power (W)			40 W (8 W × 5 lamps)		

2.4. Measurement of the Degradation of the PA66 Microfibres

2.4.1. Mass Loss

A common method to quantify the photocatalytic degradation of plastics is to evaluate the percentage of mass loss [39,43,44]. The percentage of mass loss can be determined using Equation (1) as described in [40]:

$$Mass\ Loss\ (\%) = \frac{(m_0 - m)}{m_0} \times 100 \quad (1)$$

where m_0 represents initial mass of the fibre (mg) before the experiment and m corresponds to the final mass (mg) after the experiment. The evolution of mass of fibre with time can be used to determine the kinetics of the photocatalytic degradation of the MPs. The Langmuir–Hinshelwood (L–H) and first-order expressions have been widely used to explain the kinetics of photocatalytic reactions [45–47]. The photocatalytic degradation can be quantitatively estimated by comparing the apparent reaction rate constants (κ_{app}) obtained from the first-order rate equation derived from the L–H model as Equation (2) as described in [47].

$$\ln(C/C_0) = -\kappa_{app} t \quad (2)$$

where C_0 is the initial concentration of the organic compound (mg/L), in this case it will be approximated to the amount of suspended fibres per volume of water; C is the concentration of fibre at a particular time of the photocatalytic reaction (mg/L); κ_{app} is the apparent rate constant of the reaction, and t is the irradiation time. The values of κ_{app} can be obtained from the linear regression analysis in the plot [48,49]. The κ_{app} quantifies the rate of a reaction and the higher κ_{app} indicates the faster degradation of the original organic compound.

The reaction constant i.e., half-life, which is the time that the initial concentration of reactant is decreased to one-half of its initial value, can be calculated using Equation (3) as described in [50].

$$t_{1/2} = \ln(2)/k \quad (3)$$

The mass loss observed was also used to estimate the kinetics of the photocatalytic degradation of PA66 microfibres.

2.4.2. Morphological Properties of PA66 Microfibres

A scanning electron microscope (SEM) Supra 55VP, ZEISS, Germany was used to assess the degradation of polymers. The PA66 microfibres were placed on an aluminium stub using conductive

and adhesive carbon tape cut into 0.5 × 0.5 cm. The samples were pretreated with platinum using a vacuum coater (EM ACE200, Leica, Germany) with a sputter current of 20 mA for 100 s.

2.4.3. Surface Chemistry of the PA66 Microfibres

During the photodegradation of polymer, different chemical groups, mainly carbonyl and hydroxyl groups, can be formed [51]. The carbonyl index (*CI*) (see Equation (4)) was measured from the Fourier Transform Infrared (FTIR) spectra from the fibres and it was used to monitor the oxidation of their surface [35,49,52]. *CI* can be defined as the ratio between carbonyl signal and a reference band from methylene.

$$Carbonyl\ Index\ (CI) = \frac{Absorbance\ (carbonyl\ band)}{Absorbance\ (reference\ band)} \quad (4)$$

The absorbance of the carbonyl band generally falls between 1900 and 1600 cm^{-1} and the reference peak can be the CH_3 rocking band or the CH_2 scissoring band which correspond to vibrations of groups not affected by oxidation [44,51–54]. High *CI* indicates a high degree of polymer degradation [53].

To analyse the changes in chemical properties due to the degradation mechanisms, FTIR spectroscopy (Nicolet 6700, Thermo Scientific, Waltham, MA, USA) was used. The transmittance within the wavenumber 650–4000 cm^{-1}, with a resolution of 8 cm^{-1}, was measured. The FTIR spectra were obtained in attenuated total reflectance (ATR) mode by placing the PA66 microfibre samples (SP1 to SP6) directly below the zinc selenide diamond prism without any pretreatment. Spectra were auto corrected with auto base function.

2.4.4. Monitoring the Degradation of the Suspension of PA66 Fibres with the Analysis of the Chemical Oxygen Demand (COD) in Solution

COD was used to evaluate the degree of mineralization and formation of by-products during the degradation of organic pollutants [47]. COD was measured with a spectrophotometer (DR2800, Hach, Loveland, CO, USA) as follows. The water samples in SP1 to SP6 were collected in 10 mL glass vials, where particles were left to settle for 24 h. The supernatant (2 mL) was separated and placed in digestion glass vials (TNTplus™, Hach, Loveland, CO, USA). The digestion glass vials (now containing digestion solution and the supernatant of samples) were manually shaken for 1 min to mix them thoroughly well and placed into the heater (HS-R200, HUMAS, Daejeon, South Korea) at 150 °C for 2 h. Afterwards, the vials were cooled at room temperature for 1 h, and then the vials were wiped to remove any fingerprints or dirt before placing them into the holder of spectrophotometer for analysis. The COD was determined using low range digest reagent (LR, TNT 3-150, Hach, USA) measuring from 3 to 150 mg/L. COD tests were carried out in triplicate.

3. Results and Discussion

3.1. Effect of UV Irradiation and Catalyst on the Kinetics of the Photocatalytic Degradation of PA66 Microfibres

Figure 6 shows the mass loss of the PA66 microfibre samples (SP1 to SP6) exposed to different combinations of UV irradiation and catalyst for 105 h. The effects of UV wavelengths were investigated by comparing photo-oxidation under UVA (SP3) and UVC (SP5). While the mass loss of SP5 was 83%, SP3 had only 6% mass loss within 105 h of reaction time (precision for these experiments was <28% for SP3 and <14% for SP5). Therefore, it is evident that the short wavelength (UVC) was more effective than the long wavelength (UVA) in degrading PA66 and this agrees well with other studies investigating the degradation of polyamide [55–63]. This result may potentially be explained by different intermediate products forming from the polymer by the action of UVA and UVC with possible different degradation mechanisms [63].

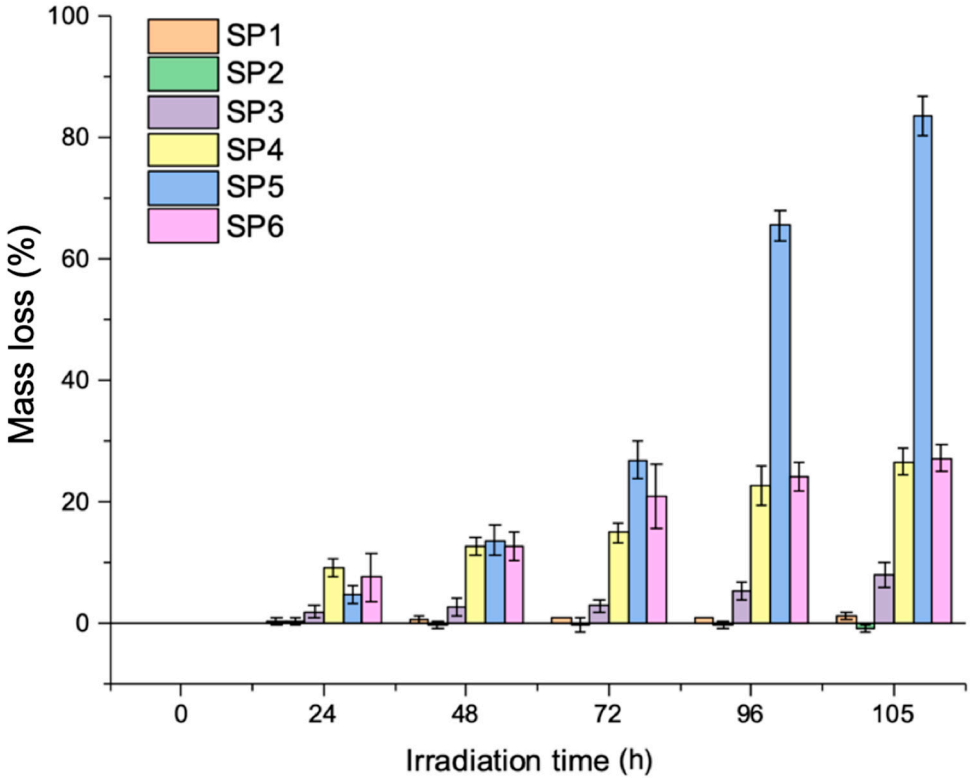

Figure 6. Experiment investigating the degradation of the PA66 microfibres under different conditions of UV and presence of catalyst for 105 h. SP1 = *deionised water*; SP2 = *deionised water* + TiO_2; SP3 = *deionised water* + UVA; SP4 = *deionised water* + UVA + TiO_2; SP5 = *deionised water* + UVC; SP6 = *deionised water* + UVC + TiO_2. Error bars = standard deviation of a triplicate study. The average initial mass of the PA66 microfibres used was 1.26 mg.

Compared to the mass loss by photo-oxidation under UVC (SP5, 83%) without including catalyst, photocatalysis using TiO_2 under UVA (SP4, 26%) and UVC (SP6, 24%) showed both lower mass loss (p 0.05). This result is not in agreement with a study that found that photocatalysis led to greater mass loss (of polyethylene in that case) [64]. It might be possible that the concentration of TiO_2 (1 g in 50 mL) was excessive and blocked the light from reaching the surface of the polymer [65]. It was suggested that the initial photocatalytic reaction rate was directly proportional to the mass of catalysts but this may be the case for a limited photocatalyst concentration range [66]. Therefore, the study conditions with high dose of catalyst (2%), have caused photocatalysis with low effectivity compared to photo-oxidation resulting in decelerating the degradation rate.

Under hydration conditions (SP1), the mass loss of the fibres was minimal (2%) for all reaction times studied (see Figure 6), and where there was absence of UV irradiation (SP2), the mass of the microfibres increased by 0.7% due to the adsorbed TiO_2 particles to the microfibres as observed in the SEM micrographs in Figure 10c. Based on these results, the effects of hydration and adsorption of TiO_2 onto fibres, both without using UV, are negligible at degrading the PA66 microfibres within 105 h. However, temperature might have favoured the degradation of the microfibres. The authors of [67] found that photolysis with increased temperature reduced dissolved organic carbon (DOC). Therefore, it is recommended to investigate the effect of temperature on microfibre degradation.

The apparent reaction rate constant (κ_{app}) and the half-life ($t_{1/2}$) in Table 3 were calculated from the $\ln(C/C_0)$ versus time plots in Figure 7. Given that greater κ_{app} refers to greater degradation rate of microfibres, it can be confirmed that SP5 presented the highest degradation rate as 13.6×10^{-3} h^{-1} followed by SP6 (2.6×10^{-3} h^{-1}) and SP4 (2.3×10^{-3} h^{-1}) which is consistent with the mass loss data. The half-life of SP5 was 51 h (see Table 3) which indicates that the initial concentration of the polymer

(1.26 mg/50 mL) would be reduced to its half (0.63 mg/50 mL) after 51 h. The short UV wavelength was more effective at degrading PA66 microfibres compared to the longer wavelength, excluding the role of TiO_2. However, applying photo-oxidation in WWTPs would have low practicality as it would take at least 51 h to degrade half of the amount of the PA66 microfibres.

Table 3. Apparent reaction constants (κ_{app}) calculated for SP1 to SP6 after 105 h of treatment. Mass loss (%) is the average result from the study carried out in triplicate.

Samples	Mass Loss (%)	Standard Deviation	κ_{app}($\times 10^3$ 1 h^{-1})	$t_{1/2}$ (h)
SP1	2	0.6	0.3	2310
SP2	0	1.2	0.1	6931
SP3	6	27.8	0.5	1733
SP4	26	0.1	2.3	301
SP5	83	14.0	13.6	51
SP6	24	0.2	2.6	267

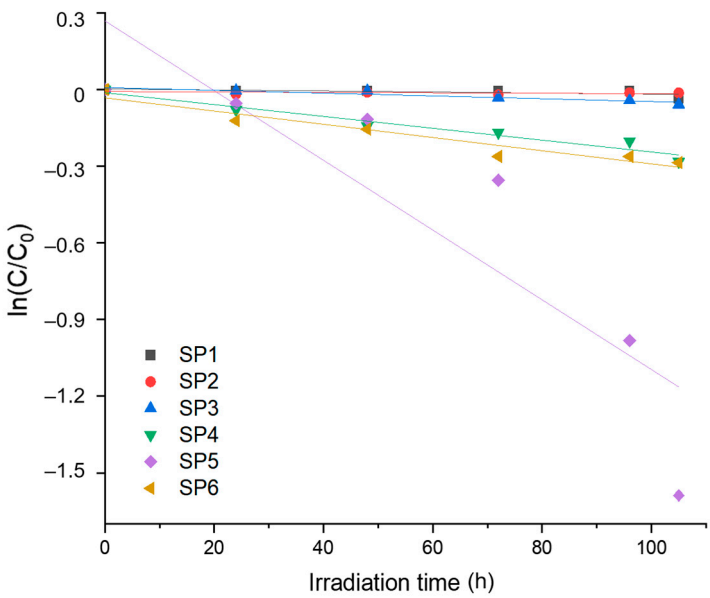

Figure 7. Evaluation of the apparent reaction rate constant (κ_{app}) of SP1–SP6.

3.2. Mass Loss and Photocatalytic Degradation Kinetics: Effects of the Concentrations of Catalysts

To assess the effects of the concentration of the catalyst on the degradation rate of PA66 microfibres, a second experiment was performed to test the effect of different doses of TiO_2 (up to 20 g/L) under UVC for 45 h. As shown in Figure 8, the conditions tested in SPT2 (100 mg TiO_2/L) showed 97% of mass loss in 48 h, followed by 78% for SPT3 (500 mg TiO_2/L) and 24% for SPT4 (1000 mg TiO_2/L) while SPT1 (no TiO_2) and SPT5 (20,000 mg TiO_2/L) resulted in the least mass loss of 18% and 14%, respectively. Hence, the maximum (SPT5) and minimum (SPT1) TiO_2 concentrations led to the lowest fibre mass loss, which is in agreement with an earlier study finding that the concentration of TiO_2 outside a particular concentration range can deaccelerate the degradation [68]. Although the most effective degradation was photo-oxidation under UVC (SP5) in Figure 6—as the amount of TiO_2 for SP6 was excessive and unoptimised—Figure 8 shows that photocatalysis is the most effective approach for degrading microfibres when the amount of TiO_2 is optimised (SPT2).

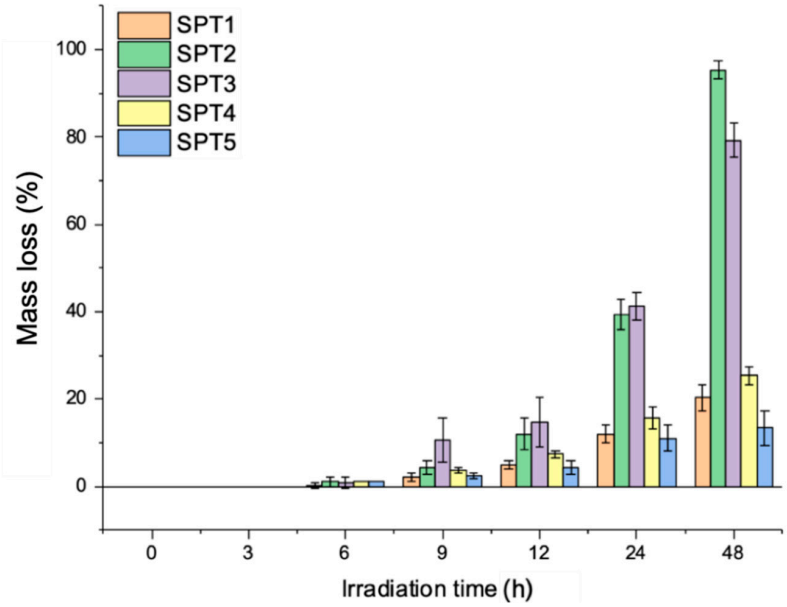

Figure 8. Degradation of PA66 microfibres under UVC with different concentrations of catalyst for 48 h. SPT1 = TiO_2 (0 mg/L); SPT2 = TiO_2 (100 mg/L); SPT3 = TiO_2 (500 mg/L); SPT4 = TiO_2 (1000 mg/L); SPT5 = TiO_2 (20,000 mg/L). Error bars = standard deviation of a triplicate. The average initial mass of the PA66 microfibres was 1.27 mg.

The κ_{app} was determined from the ln(C/C_0) versus time plots in Figure 9. Half-lives ($t_{1/2}$ (h)) are indicated in Table 4. SPT2 showed the highest constant (7.0×10^{-2} h^{-1}) while SPT5 showed the lowest constant (0.3×10^{-2} h^{-1}). Therefore, these results confirmed that the TiO_2 at 100 mg/L is the most effective condition for the PA66 degradation. Moreover, it can be confirmed that the excessive addition of TiO_2 can hinder the degradation as SPT5, leading to a lower kinetic constant compared to the SPT1, which contained no catalyst. Since SPT2 showed 10 h of fibres' half-life, these conditions could potentially be applied in the WWTPs to treat microfibres, although careful examination of the degradation products, including possible yield of nanofibres from the degradation needs to be done.

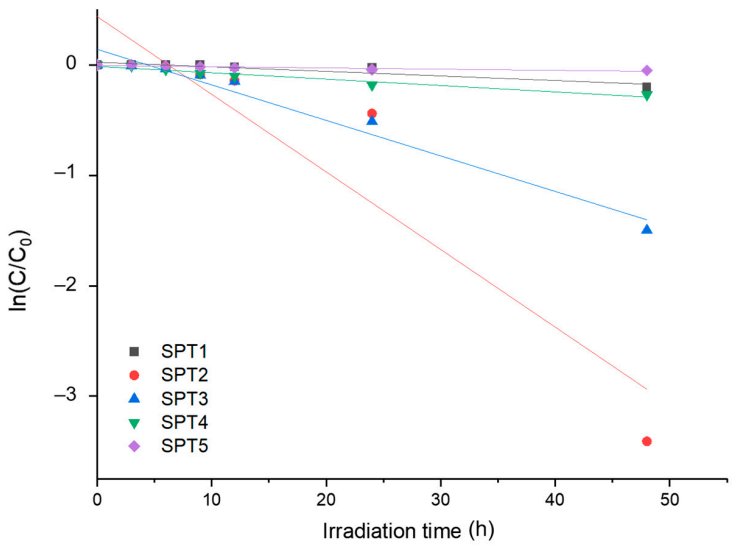

Figure 9. ln(C/C_0) versus time plots for the evaluation of the rate constant (κ_{app}) for 48 h. SPT1 = TiO_2 (0 mg/L); SPT2 = TiO_2 (100 mg/L); SPT3 = TiO_2 (500 mg/L); SPT4 = TiO_2 (1000 mg/L); SPT5 = TiO_2 (20,000 mg/L). Note that the red circles for SPT2 are overlapping with another symbol.

Table 4. Apparent reaction constant (κ_{app}) and half-life ($t_{1/2}$) calculated for SPT1 to SPT5, where different concentrations of TiO_2 from 0 to 20,000 mg/L were used.

Samples	TiO_2 (mg/L)	Mass Loss (%)	Standard Deviation (n = 3)	κ_{app} ($\times 10^2$ 1 h^{-1})	$t_{1/2}$ (h)
SPT1	0	18	1.3	0.4	173
SPT2	100	97	2.0	7.0	10
SPT3	500	78	3.0	3.2	22
SPT4	1000	24	1.2	0.6	116
SPT5	20,000	14	1.5	0.3	231

3.3. Morphological Changes of Microfibres

The SEM analysis of the study microfibres, before and after oxidative treatment, was performed to examine the morphological changes of the PA66 surface due to the varying combinations of UV (A, B, and C) and TiO_2. Figure 10a is the starting PA66 microfibres (before any degradation). Figure 10b–g shows PA66 microfibres which had been exposed to the conditions of hydration, adsorption, photo-oxidation, and photocatalysis within 105 h. Clear signs of degradation can be observed in Figure 10d–g.

Figure 10b,c illustrates the effect of hydration and adsorption, respectively. Slightly eroded surface was observed from Figure 10b which is a similar phenomenon of hydrolytic degradation identified by [69–71]. The adsorption of the photocatalyst can be observed as TiO_2 particles were attached to the surface of the PA66 microfibres without any sign of cracks or damages as shown in Figure 10c.

Figure 10d,f shows the effect of photo-oxidation when UVA and UVC were irradiated, respectively. Many relatively deep cavities, cracks, and embrittled surfaces were detected from Figure 10d,f. This evidences the compromised integrity of the fibres due to the UV irradiation, which is aligned to previously reported findings of [35,68].

Figure 10e,g displays the effect of photocatalysis under UVA and UVC, respectively. The surface of the PA66 microfibre was damaged and microcracks formed. Some of the cracks were filled with TiO_2 particles. Based on this observation, it might be possible that the lower mass loss of the PA66 microfibres under photocatalysis could be due to the excessive addition of TiO_2. This is supported by previous studies [63,64]. The findings related to mass loss in this work confirm that excessive use of TiO_2 can impede the interaction of the UV irradiation with the surface of the fibres.

3.4. Changes of Chemical Properties

FTIR analysis of the PA66 microfibres was carried out to examine the changes in the chemical properties of the microfibres. The characteristic peaks of the unexposed PA66 microfibres in the FTIR spectra region are summarised in Table 5.

Figure 11 shows the characteristic FTIR spectrum of PA66 fibres which had not been exposed to any degradation mechanism. The peaks arising at 3295 and 1436 cm^{-1} can be assigned to the stretching and deformation vibration of N-H bonds; the band at 3076 cm^{-1} is associated to the stretching vibration of C-H bond; and the bands at 2917 and 2851 cm^{-1} can be due to the asymmetrical and symmetrical stretching vibration of CH_2 [71]. The stretching of the amide I (C=O stretching), amide II (C-N stretching and N-H bending), and amide III (C-N stretching) are observed at 1632, 1536, and 12,718 cm^{-1}, respectively [74]. The band located at 1141 cm^{-1} can be attributed to CCH symmetric bending vibration combined with CH_2 twisting and the bands at 933 and 682 cm^{-1} are associated with the stretching and bending vibration of C-C bonds [69,73]. The increase of the intensity of a band from an oxidised group such as carbonyl (C=O), with respect to a reference peak within the same spectrum, can indicate that there are more oxygenated groups after the treatment compared to the initial state; therefore, the FTIR spectrum can be used to assess the level of oxidation.

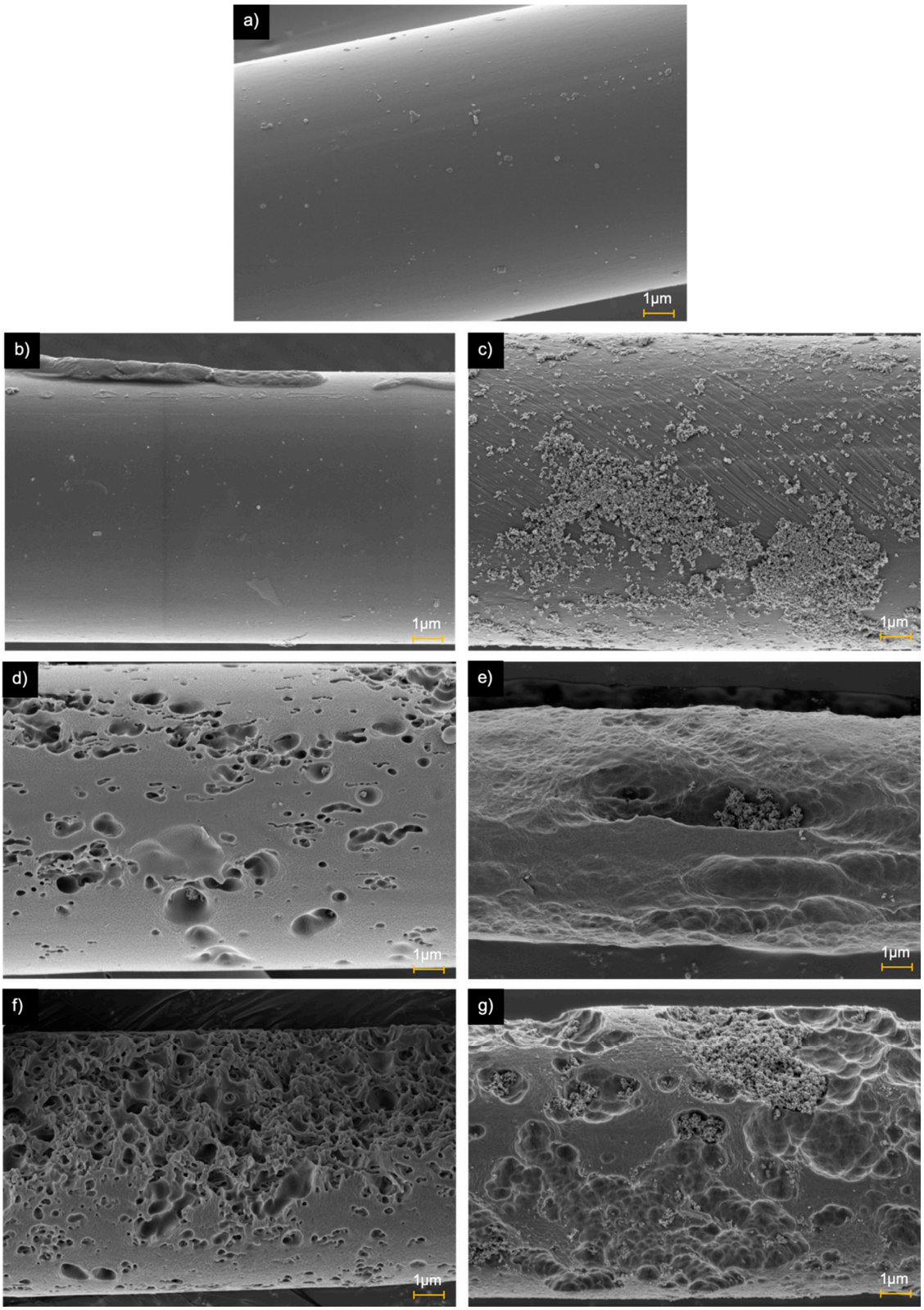

Figure 10. SEM micrograph of PA66 microfibres after different degradation conditions were applied for 105 h: (**a**) starting PA66 microfibres, (**b**) PA66 microfibres that had been suspended in deionised water; (**c**) in deionised water + TiO_2, (**d**) in deionised water + UVA; (**e**) in deionised water + UVA + TiO_2, (**f**) in deionised water + UVC, (**g**) in deionised water + UVC + TiO_2. All images are taken at a magnification of 20.00 K.

Table 5. FTIR assignment of bands observed in PA66 fibres with the wavenumber and type of signal. Adapted from [72–75].

Wavenumber (cm^{-1})	Intensity *	Assignment
3295	M	N-H stretching
3076	W	C-H stretching
2918	MS	CH_2 stretching (asymmetrical)
2851	MS	CH_2 stretching (symmetrical)
1632	VS	Amide I (C=O stretching)
1535	VS	Amide II (C-N stretching and N-H bending)
1463	S	N-H deformation/CH_2 scissoring
1271	S	Amide III (C-N stretching)
1141	M	CCH symmetric bending/CH_2 twisting
933	M	C-C stretching
681	VS	C-C bending

* VS—very strong; S—strong; MS—medium strong; M—medium; W—weak.

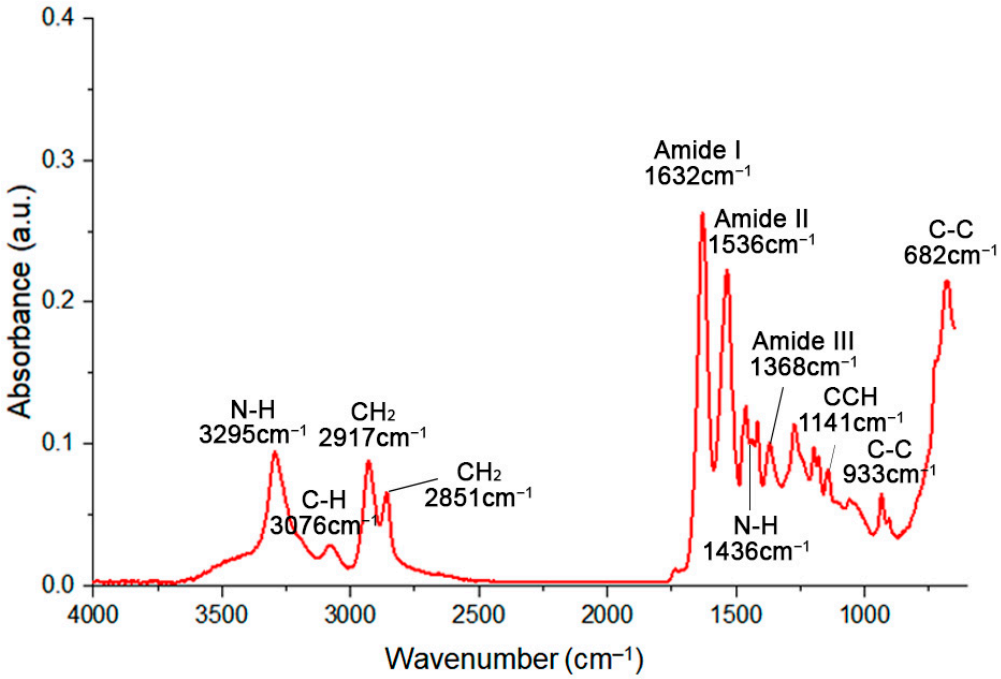

Figure 11. FTIR band assignment of PA66 microfibres unexposed to degradation mechanism.

The band ≈1630 cm^{-1} may correspond to the carbonyl group from amide groups (NH-C=O) and the reference peak selected was the most intense band from the CH_2 stretching. The reference blank was selected assuming that CH groups may undergo less oxidation and may remain constant [76]. (Figure 12).

Using Equation (4), *CI* values for the SP1 to SP6 were calculated as summarised in Table 6. The *CI* values were converted into the percentage increase compared to the starting fibres. The results showed that the photo-oxidation under UVC (SP5, 27%), photocatalysis under UVC (SP6, 25%), and photo-oxidation under UVA (SP4, 19%) led to higher oxidation degree compared to the unexposed PA66 microfibres (SP1, 0%). The different level of oxidation due to the UVC and UVA might be due to the different energies of the radiation and intermediate products generated during the photodegradation depending on the long and short wavelengths [63]. However, no change in absorbance in the region

near 3500 cm^{-1} was detected in the experiment which indicates that the presence of hydroxyl groups did not tend to increase much throughout the conditions tested. This result corroborates well with the result elsewhere [77] and it is in agreement with the no generation of alcohols and carboxylic acid during the photo-oxidation and photocatalytic degradation of PA66 microfibres.

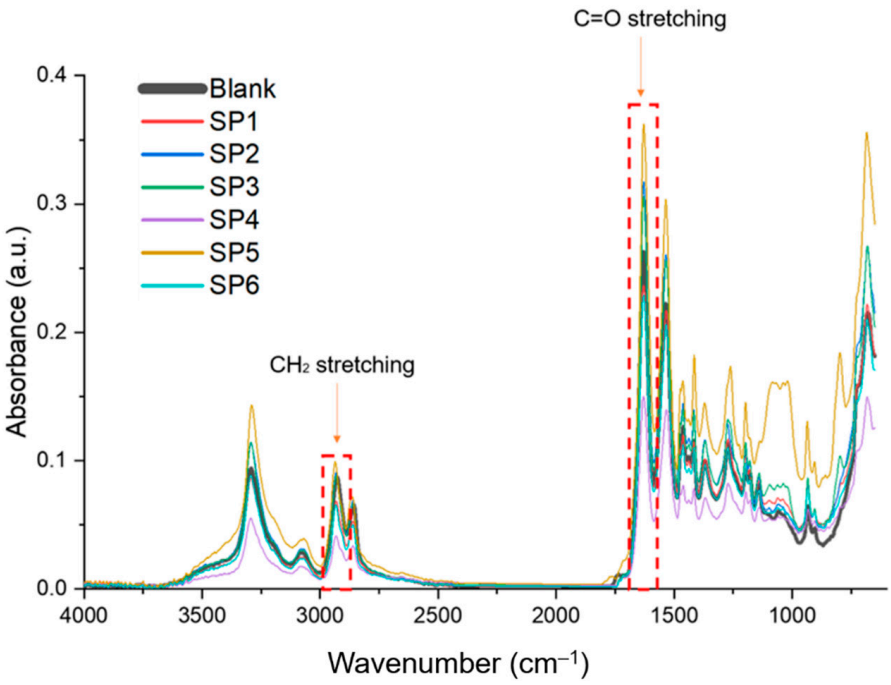

Figure 12. FTIR spectra of PA66 microfibres before (blank) and after the treatment (SP1-SP6) with different conditions of UV and TiO_2. SP1 = deionised water; SP2 = deionised water + TiO_2; SP3 = deionised water + UVA; SP4 = deionised water + UVA + TiO_2; SP5 = deionised water + UVC; SP6 = deionised water + UVC + TiO_2. a.u—arbitrary units.

Table 6. Carbonyl index (CI) of unexposed PA66 microfibres (starting fibres) and PA66 microfibres exposed to different UV and TiO_2 conditions (SP1 to SP6) for 105 h.

Degradation Conditions	Carbonyl Index [C=O:CH_2]	Percentage Increase of C=O Compared to the Starting Fibre (%)
Starting fibre	2.68	0
SP1	3.05	14
SP2	3.13	17
SP3	3.17	18
SP4	3.18	19
SP5	3.40	27
SP6	3.35	25

3.5. Formation of By-Products Due to the Degradation of PA66 Microfibres

To assess by-products generated due to the degradation mechanisms of hydration, adsorption, photo-oxidation, and photocatalytic degradation, the COD of the water where the fibres were suspended was measured (Table 7). SPW1 to SPW6 refer to the water sample taken from SP1 to SP6 where the PA66 microfibres were exposed to different UV and catalyst conditions (given in Table 7). R-DW refers to the reference deionised water without microfibers. R-TiO_2 refers to 20,000 mg/L of TiO_2 in water without UV irradiation.

COD was below the limit of detection (3.4 mg/L in R-DW). In contrast, COD was 40 mg/L (when measuring the solution that contained suspended TiO_2 and no presence of microfibres (R-TiO_2). These latter results could be the effect of residual TiO_2 on the measurement.

Table 7. The COD of the water were the PA66 microfibres were suspended and exposed to the different conditions of UV and catalyst (SPW1–SPW6). R-DW refer to the reference water sample; R-TiO_2 refers to 20,000 mg/L of TiO_2 in water without UV irradiation. COD results were averaged from the triplicate data.

Water Sample	Presence of Microfibres	Effect	Degradation Condition	COD (mg/L) ±SD, n = 3	Mass Loss (%)
R-DW	No	Reference	Deionised water + No light	<LOD	-
R-TiO_2	No	Reference	Deionised water + TiO_2 + No light	40.0 ± 10.4	-
SPW1	Yes	Hydration	Deionised water + No light	14.7 ± 9.0	2
SPW2	Yes	Adsorption	Deionised water + TiO_2 + No light	30.3 ± 8.5	0
SPW3	Yes	Photo-oxidation	Deionised water + UVA	30.0 ± 1.0	6
SPW4	Yes	Photocatalysis	Deionised water + UVA + TiO_2	7.7 ± 4.5	26
SPW5	Yes	Photo-oxidation	Deionised water + UVC	30.7 ± 7.5	83
SPW6	Yes	Photocatalysis	Deionised water + UVC + TiO_2	10.0 ± 4.0	24

The lowest COD levels. LOD (limit of detection) estimated at 3.4 mg/L. SD is standard deviation.

Water from the photocatalysis experiments (SPW4 and SPW6) showed relatively low COD compared to the water from adsorption (SPW2), and photo-oxidation (SPW3 and SPW5) experiments (see Table 7). Although the difference is not significant, the COD level decreased the most when TiO_2 and UV irradiation are applied simultaneously in this experiment. The released of oxidised parts of the fibre due to the photo-induced reaction could be the cause of the increased COD observed. These results (SPW4 and SPW6) demonstrate the degradability of PA66 microfibres with photocatalytic degradation while generating a low level of COD. Thus, the photocatalytic degradation can potentially be applicable to WWTPs without violating the discharge compliance of COD. However, it is recommended to examine the presence of nanofibres or debris with SEM or transmission electron microscopy (TEM) and systems able to detect the particle size distribution in the suspended solution (e.g., nanosizer).

3.6. Insights to Microfibre-Targeted Treatment Technology

Photocatalysis of PA66 microfibres suspended in water using UVC with 100 mg/L of TiO_2 resulted in 97% of mass loss in 48 h (Figure 6)with a relatively low level of COD. This suggests low formation of degradation by-products during the treatment and it could a potential technology to treat microfibres in WWTPs. Although this work is a preliminary study, the proposed photocatalysis might not be suitable for a stand-alone process as UV treatment is not effective for treating high turbidity water. However, it could be developed as tertiary treatment for microfibre residuals which could not be completely removed by the secondary wastewater treatment. Additionally, potential microfibre residuals in drinking water after coagulation-flocculation, flotation, or filtration could be removed by photocatalysis. However, a more detailed investigation is suggested about by-products generated, matrix effect, energy required by the process, and effect of temperature. Concerns regarding the use of slurry type of TiO_2 in photocatalytic treatment can be overcome by the application of a hybrid coagulation step as suggested elsewhere [37].

The development of microfibre-targeted treatment technologies will benefit the health of humans and the ecosystem by preventing the release of microfibres into the environment if the treatment process does not lead to nanofibres. Further investigation is required to develop photocatalysis as a microfibre-targeted technology, the present study successfully demonstrated the degradation of PA66 microfibres using photocatalysts suspended ultrapure water. Therefore, it provides new insights on the degradation of microfibres by AOPs and open horizons for future research.

4. Conclusions

PA66 microfibres can be degraded with photocatalysis. The optimal conditions for the degradation of PA66 microfibres in ultrapure water were under UVC with 100 mg/L of TiO_2. Under these conditions, 97% of average mass loss was achieved within 48 h. Photocatalysis generated low level of fibre by-products compared to photo-oxidation. The result indicates that photocatalysis can degrade PA66 microfibres in WWTPs while there is a need to further assess the products generated from the degradation of the microfibres. The present study is a pioneer investigation on the degradation of PA66 microfibres using photo-oxidation and photocatalysis. The main findings of this research are as follows:

- The degradation of PA66 microfibres was dependent on the wavelengths of UV irradiation during the photo-oxidation. The degradation was more effective when using a short wavelength (254 nm) (approximately 14 times more effective in degrading PA66 microfibres compared to using 365 nm).
- The concentration of TiO_2 was an important factor in accelerating the degradation rate of PA66 microfibres. The optimal concentration in this study was 100 mg TiO_2/L.
- The photocatalytic degradation of PA66 microfibres generated organic by-products, but it was relatively low compared to photo-oxidation.

The photo-oxidation under UVC was the most effective treatment as 83% of microfibres' mass loss was achieved in 105 h; UVC was more effective than UVA in degrading the microfibres (UVA only achieved 6% of mass loss during the photo-oxidation). The effects of hydration and adsorption were negligible as the mass loss of the sample non exposed to light was <2%. The *CI* was greatest (hence maximum oxidation) at 3.40 for the PA66 microfibres that had been photo-oxidised under UVC which is equivalent to a 27% increase of oxidation level compared to the PA66 microfibres unexposed to any degradation mechanisms. The mass loss results were in agreement with the *CI* under photo-oxidation by UVC.

SEM analysis showed microcracks and cavities on the surface of the microfibres, confirming the degradation effect of photo-oxidation and photocatalysis thereof. The COD was relatively low when the photocatalysis was applied (<10 mg COD/L) compared to the effect of photo-oxidation (>30 mg/L). The most effective concentration of TiO_2 was 100 mg/L, which lead to 97% of mass of microfibres lost in 48 h. The half-life of fibres in SP6 (concentration of TiO_2 as 20,000 mg/L under UVC), was reduced from 267 to 10 h when 100 mg/L TiO_2 concentration was applied (SPT2).

The present study demonstrated the effects of UV and TiO_2 in photo-oxidation and photocatalytic degradation of PA66 microfibres in ultrapure water. Therefore, these results provide new insights for applying the photocatalysis as a microfibre-targeted treatment technology in WWTPs with minimal generation of by-products in terms of COD. However, future research should be carried out considering the potential effects of (1) applying different types of microfibres such as PS and PET; (2) testing different conditions such as applying stirrer in the reaction chamber, adjusting pH level and temperature, and using different types of catalyst; (3) assessing the photocatalysis with realistic water sampled from secondary effluent of WWTPs; (4) investigating the formation of by-products comprehensively, such as identifying the generation of nanoparticles and other potential intermediate compounds dissolved in the water.

Author Contributions: Conceptualization, J.-M.L. and L.C.C.; Methodology, J.-K.K., J.-M.L., and S.-H.L.; Analysis, J.-M.L. and I.-C.C.; Interpretation, J.-M.L. and R.B.; Supervision, L.C.C.; Project administration, L.C.C.; Writing—Original Draft Preparation, J.-M.L.; Writing—Review and Editing, I.-C.C., J.-K.K., L.C.C., R.B., and S.-H.L. All authors have read and agreed to the published version of the manuscript.

Funding: This work was supported by the National Research Foundation of Korea (NRF) grant funded by the Korea government (MSIT) (No. 2019R1F1A1060666).

Conflicts of Interest: The authors declare no conflict of interest.

References

1. Avio, C.G.; Gorbi, S.; Regoli, F. Plastics and microplastics in the oceans: From emerging pollutants to emerged threat. *Mar. Environ. Res.* **2017**, *128*, 2–11. [CrossRef]
2. Alimba, C.G.; Faggio, C. Microplastics in the marine environment: Current trends in environmental pollution and mechanisms of toxicological profile. *Environ. Toxicol. Pharm.* **2019**, *68*, 61–74. [CrossRef]
3. Geyer, R.; Jambeck, J.R.; Law, K.L. Production, use, and fate of all plastics ever made. *Sci. Adv.* **2017**, *3*, e1700782. [CrossRef]
4. Browne, M.A.; Crump, P.; Niven, S.J.; Teuten, E.; Tonkin, A.; Galloway, T.; Thompson, R. Accumulation of microplastic on shorelines woldwide: Sources and sinks. *Environ. Sci. Technol.* **2011**, *45*, 9175–9179. [CrossRef]
5. Boucher, J.; Friot, D. *Primary Microplastics in the Oceans: A Global Evaluation of Sources*; IUCN: Gland, Switzerland, 2017. [CrossRef]
6. Peller, J.R.; Eberhardt, L.; Clark, R.; Nelson, C.; Kostelnik, E.; Iceman, C. Tracking the distribution of microfiber pollution in a southern Lake Michigan watershed through the analysis of water, sediment and air. *Environ. Sci. Process. Impacts* **2019**, *21*, 1549–1559. [CrossRef]
7. Singh, R.P.; Mishra, S.; Das, A.P. Synthetic microfibers: Pollution toxicity and remediation. *Chemosphere* **2020**, *257*, 127199. [CrossRef]
8. GESAMP. *Sources, Fate and Effects of Microplastics in the Marine Environment: A Global Assessment*; IMO: London, UK, 2015; Volume 90, p. 96. [CrossRef]
9. Hartmann, N.B. Are We Speaking the Same Language? Recommendations for a Definition and Categorization Framework for Plastic Debris. *Environ. Sci. Technol.* **2019**, *53*, 1039–1047. [CrossRef]
10. Barnes, D.K.A.; Galgani, F.; Thompson, R.C.; Barlaz, M. Accumulation and fragmentation of plastic debris in global environments. *Philos. Trans. R. Soc. B Biol. Sci.* **2009**, *364*, 1985–1998. [CrossRef]
11. Cárdenas, A.M.; Halloran, J.O.; van Pelt, F.N.A.M.; Jansen, M.A.K. Rapid fragmentation of microplastics by the freshwater amphipod Gammarus duebeni (Lillj.). *Sci. Rep.* **2020**, *10*, 1–12. [CrossRef]
12. Foley, C.J.; Feiner, Z.S.; Malinich, T.D.; Höök, T.O. A meta-analysis of the effects of exposure to microplastics on fish and aquatic invertebrates. *Sci. Total Environ.* **2018**, *631–632*, 550–559. [CrossRef]
13. Au, S.Y.; Bruce, T.F.; Bridges, W.C.; Klaine, S.J. Responses of Hyalella azteca to acute and chronic microplastic exposures. *Environ. Toxicol. Chem.* **2015**, *34*, 2564–2572. [CrossRef]
14. Ogonowski, M.; Schür, C.; Jarsén, Å.; Gorokhova, E. The Effects of Natural and Anthropogenic Microparticles on Individual Fitness in Daphnia magna. *PLoS ONE* **2016**, *11*. [CrossRef]
15. Sussarellu, R.; Suquet, M.; Thomas, Y.; Lambert, C.; Fabioux, C.; Pernet, M.E.J.; Corporeau, C. Oyster reproduction is affected by exposure to polystyrene microplastics. *Proc. Natl. Acad. Sci. USA* **2016**, *113*, 2430–2435. [CrossRef]
16. Booth, A.M.; Hansen, B.H.; Frenzel, M.; Johnsen, H.; Altin, D. Uptake and toxicity of methylmethacrylate-based nanoplastic particles in aquatic organisms. *Environ. Toxicol. Chem.* **2016**, *35*, 1641–1649. [CrossRef]
17. Besseling, E.; Wegner, A.; Foekema, E.M.; van den Heuvel-Greve, M.J.; Koelmans, A.A. Effects of microplastic on fitness and PCB bioaccumulation by the lugworm Arenicola marina (L.). *Environ. Sci. Technol.* **2013**, *47*, 593–600. [CrossRef]
18. Dalberg, A.; de Wit, W.; Bigaud, N. *Assessing Plastic Ingestion from Nature to People (AN ANALYSIS for WWF)*; The University of New Castle: Callaghan, Australia, 2019.
19. Liebmann, B.; Köppel, S.; Philipp, K.; Theresa, B.; Thomas, R.; Philipp, S. Assessment of microplastic concentrations in human stool final results of a prospective study. *Conf. Nano Microplastics Tech. Freshw. Syst. Microplastics* **2018**, 28–31. [CrossRef]
20. von Moos, N.; Burkhardt-Holm, P.; Köhler, A. Uptake and effects of microplastics on cells and tissue of the blue mussel Mytilus edulis L. after an experimental exposure. *Environ. Sci. Technol.* **2012**, *46*, 11327–11335. [CrossRef]
21. Zhang, Q.; Xu, E.G.; Li, J.; Chen, Q.; Ma, L.; Zeng, E.Y.; Shi, H. A Review of Microplastics in Table Salt, Drinking Water, and Air: Direct Human Exposure. *Environ. Sci. Technol.* **2020**, *54*, 3740–3751. [CrossRef]
22. Oberbeckmann, S.; Löder, M.G.J.; Labrenz, M. Marine microplastic-associated biofilms—A review. *Environ. Chem.* **2015**, *12*, 551–562. [CrossRef]
23. Bergmann, M.; Gutow, L.; Klages, M. Marine anthropogenic litter. *Mar. Anthr. Litter.* **2015**, 1–447. [CrossRef]

24. Prata, J.C. Microplastics in wastewater: State of the knowledge on sources, fate and solutions. *Mar. Pollut. Bull.* **2018**, *129*, 262–265. [CrossRef]
25. Murphy, F.; Ewins, C.; Carbonnier, F.; Quinn, B. Wastewater Treatment Works (WwTW) as a Source of Microplastics in the Aquatic Environment. *Environ. Sci. Technol.* **2016**, *50*, 5800–5808. [CrossRef]
26. Xu, X.; Hou, Q.; Xue, Y.; Jian, Y.; Wang, L.P. Pollution characteristics and fate of microfibers in the wastewater from textile dyeing wastewater treatment plant. *Water Sci. Technol.* **2018**, *78*, 2046–2054. [CrossRef]
27. Ziajahromi, S.; Neale, P.A.; Rintoul, L.; Leusch, F.D.L. Wastewater treatment plants as a pathway for microplastics: Development of a new approach to sample wastewater-based microplastics. *Water Res.* **2017**, *112*, 93–99. [CrossRef]
28. Magnusson, K.; Norén, F. Screening of Microplastic Particles in and Down-Stream a Wastewater Treatment Plant. Available online: www.ivl.se (accessed on 25 June 2020).
29. McCormick, A.; Hoellein, T.J.; Mason, S.A.; Schluep, J.; Kelly, J.J. Microplastic is an abundant and distinct microbial habitat in an urban river. *Environ. Sci. Technol.* **2014**, *48*, 11863–11871. [CrossRef]
30. Hanvey, J.S.; Lewis, P.J.; Lavers, J.L.; Crosbie, N.D.; Pozo, K.; Clarke, B.O. A review of analytical techniques for quantifying microplastics in sediments. *Anal. Methods* **2017**, *9*, 1369–1383. [CrossRef]
31. Okoffo, E.D.; O'Brien, S.; O'Brien, J.W.; Tscharke, B.J.; Thomas, K.V. Wastewater treatment plants as a source of plastics in the environment: A review of occurrence, methods for identification, quantification and fate. *Environ. Sci. Water Res. Technol.* **2019**, *5*, 1908–1931. [CrossRef]
32. Li, C.; Busquets, R.; Campos, L.C. Assessment of microplastics in freshwater systems: A review. *Sci. Total Environ.* **2020**, *707*. [CrossRef]
33. Bratovcic, A. Degradation of Micro- and Nano-Plastics by Photocatalytic Methods. *J. Nanosci. Nanotechnol. Appl.* **2017**, *3*, 1–9. [CrossRef]
34. Brienza, M.; Katsoyiannis, I.A. Sulfate radical technologies as tertiary treatment for the removal of emerging contaminants from wastewater. *Sustainability* **2017**, *9*, 1604. [CrossRef]
35. Tofa, T.S.; Kunjali, K.L.; Paul, S.; Dutta, J. Visible light photocatalytic degradation of microplastic residues with zinc oxide nanorods. *Environ. Chem. Lett.* **2019**, *17*, 1341–1346. [CrossRef]
36. Liu, P.; Qian, L.; Wang, H.; Zhan, X.; Lu, K.; Gu, C.; Gao, S. New Insights into the Aging Behavior of Microplastics Accelerated by Advanced Oxidation Processes. *Environ. Sci. Technol.* **2019**, *53*, 3579–3588. [CrossRef]
37. Thiruvenkatachari, R.; Vigneswaran, S.; Moon, I.S. A review on UV/TiO 2 photocatalytic oxidation process. *Korean J. Chem. Eng.* **2008**, *25*, 64–72. [CrossRef]
38. Li, S.; Xu, S.; He, L.; Xu, F.; Wang, Y.; Zhang, L. Photocatalytic Degradation of Polyethylene Plastic with Polypyrrole/TiO 2 Nanocomposite as Photocatalyst. *Polym. Plast. Technol. Eng.* **2010**, *49*, 400–406. [CrossRef]
39. Ariza-Tarazona, M.C.; Villarreal-Chiu, J.F.; Barbieri, V.; Siligardi, C.; Cedillo-González, E.I. New strategy for microplastic degradation: Green photocatalysis using a protein-based porous N-TiO 2 semiconductor. *Ceram. Int.* **2019**, *45*, 9618–9624. [CrossRef]
40. Ali, S.S.; Qazi, I.A.; Arshad, M.; Khan, Z.; Voice, T.C.; Mehmood, C.T. Photocatalytic degradation of low density polyethylene (LDPE) films using titania nanotubes. *Environ. Nanotechnol. Monit. Manag.* **2016**, *5*, 44–53. [CrossRef]
41. Tian, L.; Chen, Q.; Jiang, W.; Wang, L.; Xie, H.; Kalogerakis, N.; Ji, R. A carbon-14 radiotracer-based study on the phototransformation of polystyrene nanoplastics in water: Versus in air. *Environ. Sci. Nano* **2019**, *6*, 2907–2917. [CrossRef]
42. Thomas, R.T.; Nair, V.; Sandhyarani, N. TiO2 nanoparticle assisted solid phase photocatalytic degradation of polythene film: A mechanistic investigation. *Colloids Surf. A Physicochem. Eng. Asp.* **2013**, *422*, 1–9. [CrossRef]
43. Thomas, R.T.; Sandhyarani, N. Enhancement in the photocatalytic degradation of low density polyethylene-TiO2 nanocomposite films under solar irradiation. *RSC Adv.* **2013**, *3*, 14080–14087. [CrossRef]
44. Liang, W.; Luo, Y.; Song, S.; Dong, X.; Yu, X. High photocatalytic degradation activity of polyethylene containing polyacrylamide grafted TiO2. *Polym. Degrad. Stab.* **2013**, *98*, 1754–1761. [CrossRef]
45. Kumar, K.V.; Porkodi, K.; Selvaganapathi, A. Constrain in solving Langmuir-Hinshelwood kinetic expression for the photocatalytic degradation of Auramine O aqueous solutions by ZnO catalyst. *Dye. Pigment.* **2007**, *75*, 246–249. [CrossRef]

46. Wenhua, L.; Hong, L.; Sao'an, C.; Jianqing, Z.; Chunan, C. Kinetics of photocatalytic degradation of aniline in water over TiO2 supported on porous nickel. *J. Photochem. Photobiol. A Chem.* **2000**, *131*, 125–132. [CrossRef]
47. Rajamanickam, D.; Shanthi, M. Photocatalytic degradation of an organic pollutant by zinc oxide—Solar process. *Arab. J. Chem.* **2016**, *9*, S1858–S1868. [CrossRef]
48. Khezrianjoo, S. Langmuir-Hinshelwood Kinetic Expression for the Photocatalytic Degradation of Metanil Yellow Aqueous Solutions by ZnO Catalyst. *Chem. Sci. J.* **2012**, *2012*. [CrossRef]
49. Ariza-Tarazona, M.C.; Villareal-Chiu, J.F.; Hernández-López, J.M.; De la Rosa, J.R.; Barbieri, V.; Siligardi, C.; Cedillo-González, E.I. Microplastic pollution reduction by a carbon and nitrogen-doped TiO2: Effect of pH and temperature in the photocatalytic degradation process. *J. Hazard. Mater.* **2020**, *395*, 122632. [CrossRef]
50. Ma, Y.; Huang, A.; Cao, S.; Sun, F.; Wang, L.; Guo, H.; Ji, R. Effects of nanoplastics and microplastics on toxicity, bioaccumulation, and environmental fate of phenanthrene in fresh water. *Environ. Pollut.* **2016**, *219*, 166–173. [CrossRef]
51. Mylläri, V.; Ruoko, T.P.; Syrjälä, S. A comparison of rheology and FTIR in the study of polypropylene and polystyrene photodegradation. *J. Appl. Polym. Sci.* **2015**, *132*. [CrossRef]
52. Ahlblad, G.; Forsström, D.; Stenberg, B.; Terselius, B.; Reitberger, T.; Svensson, L.G. Oxidation profiles of polyamide 6,6 studied by imaging chemiluminescence and FTIR. *Polym. Degrad. Stab.* **1997**, *55*, 287–293. [CrossRef]
53. Krehula, L.K.; Katančić, Z.; Siročić, A.P.; Hrnjak-Murgić, Z. Weathering of high-density polyethylene-wood plastic composites. *J. Wood Chem. Technol.* **2014**, *34*, 39–54. [CrossRef]
54. Anton, A. Determination of hydroperoxides in ultraviolet-irradiated nylon 66. *J. Appl. Polym. Sci.* **1965**, *9*, 1631–1639. [CrossRef]
55. Shamey, R.; Sinha, K. A review of degradation of nylon 6.6 as a results of exposure to environmental conditions. *Rev. Prog. Color. Relat. Top.* **2003**, *33*, 93–107.
56. Chavarria, F.; Paul, D.R. Comparison of nanocomposites based on nylon 6 and nylon 66. *Polymer* **2004**, *45*, 8501–8515. [CrossRef]
57. Palmer, R.J. Polyamides, Plastics. In *Encyclopedia of Polymer Science and Technology*; John Wiley & Sons, Inc.: Hoboken, NJ, USA, 2001.
58. Taylor, H.A.; Tincher, W.C.; Hamner, W.F. Photodegradation of nylon 66. I. Phototendering by TiO2. *J. Appl. Polym. Sci.* **1970**, *14*, 141–146. [CrossRef]
59. Tang, L.; Lemaire, J.; Sallet, D. Photochemistry of Polyundecanamides. 1. Mechanisms of Photooxidation at Short and Long Wavelengths. *Macromolecules* **1982**, *15*, 1432–1437. [CrossRef]
60. Puma, G.L.; Yue, P.L. Comparison of the effectiveness of photon-based oxidation processes in a pilot falling film photoreactor. *Environ. Sci. Technol.* **1999**, *33*, 3210–3216. [CrossRef]
61. Do, C.H.; Pearce, E.M.; Bulkin, B.J. FT-IR Spectroscopic Study on the Photo- and Photooxidative Degradation of Nylons. *J. Polym. Sci. Part A Polym. Chem.* **1987**, *25*, 2301–2321. [CrossRef]
62. Stephenson, C.V.; Moses, B.C.; Burks, R.E.; Coburn, W.C.; Wilcox, W.S. Ultraviolet irradiation of plastics. II. Crosslinking and scission. *J. Polym. Sci.* **1961**, *55*, 465–475. [CrossRef]
63. Roger, A.; Sallet, D.; Lemaire, J. Photochemistry of Aliphatic Polyamides. 4. Mechanisms of Photooxidation of Polyamides 6, 11, and 12 at Long Wavelengths. *Macromolecules* **1986**, *19*, 579–584. [CrossRef]
64. Liu, G.L.; Zhu, D.W.; Liao, S.J.; Ren, L.Y.; Cui, J.Z.; Zhou, W.B. Solid-phase photocatalytic degradation of polyethylene-goethite composite film under UV-light irradiation. *J. Hazard. Mater.* **2009**, *172*, 1424–1429. [CrossRef]
65. Ghasemi, B.; Anvaripour, B.; Jorfi, S.; Jaafarzadeh, N. Enhanced Photocatalytic Degradation and Mineralization of Furfural Using UVC/TiO2/GAC Composite in Aqueous Solution. *Int. J. Photoenergy* **2016**, *2016*. [CrossRef]
66. Herrmann, J.M. Heterogeneous photocatalysis: Fundamentals and applications to the removal of various types of aqueous pollutants. *Catal. Today* **1999**, *53*, 115–129. [CrossRef]
67. Porcal, P.; Dillon, P.J.; Molot, L.A. Temperature dependence of photodegradation of dissolved organic matter to dissolved inorganic carbon and particulate organic carbon. *PLoS ONE* **2015**, *10*, 1–15. [CrossRef]
68. Saquib, M.; Muneer, M. TiO2/mediated photocatalytic degradation of a triphenylmethane dye (gentian violet), in aqueous suspensions. *Dye. Pigment.* **2003**, *56*, 37–49. [CrossRef]

69. Wiener, J.; Chládová, A.; Shahidi, S.; Peterová, L. Effect of UV irradiation on mechanical and morphological properties of natural and synthetic fabric before and after nano-TIO2 padding. *Autex Res. J.* **2017**, *17*, 370–378. [CrossRef]
70. Yousif, E.; Haddad, R. Photodegradation and photostabilization of polymers, especially polystyrene: Review. *Springerplus* **2013**, *2*, 1–32. [CrossRef]
71. Díaz-Alejo, L.A.; Menchaca-Campos, E.C.; Chavarín, J.U.; Sosa-Fonseca, R.; García-Sánchez, M.A. Effects of the addition of ortho-And para NH2 substituted tetraphenylporphyrins on the structure of nylon 66. *Int. J. Polym. Sci.* **2013**, *2013*. [CrossRef]
72. Gashti, M.P.; Assefipour, R.; Kiumarsi, A.; Gashti, M.P. Enzymatic surface hydrolysis of polyamide 6,6 with mixtures of proteolytic and lipolytic enzymes. *Prep. Biochem. Biotechnol.* **2013**, *43*, 798–814. [CrossRef]
73. Navarro-Pardo, F.; Martínez-Barrera, G.; Martínez-Hernández, A.L.; Castaño, V.M.; Rivera-Armenta, J.L.; Medellín-Rodríguez, F.; Velasco-Santos, C. Effects on the thermo-mechanical and crystallinity properties of nylon 6,6 electrospun fibres reinforced with one dimensional (1D) and two dimensional (2D) carbon. *Materials* **2013**, *6*, 3494–3513. [CrossRef]
74. Krylova, V.; Dukštienė, N. The structure of PA-Se-S-Cd composite materials probed with FTIR spectroscopy. *Appl. Surf. Sci.* **2019**, *470*, 462–471. [CrossRef]
75. Charles, J.; Ramkumaar, G.R.; Azhagiri, S.; Gunasekaran, S. FTIR and thermal studies on nylon-66 and 30% glass fibre reinforced nylon-66. *E-J. Chem.* **2009**, *6*, 23–33. [CrossRef]
76. Moezzi, M.; Yekrang, J.; Ghane, M.; Hatami, M. The effects of UV degradation on the physical, thermal, and morphological properties of industrial nylon 66 conveyor belt fabrics. *J. Ind. Text.* **2019**, 240–260. [CrossRef]
77. El Mazry, C.; Hassine, M.B.; Correc, O.; Colin, X. Thermal oxidation kinetics of additive free polyamide 6-6. *Polym. Degrad. Stab.* **2014**, *98*, 22–36. [CrossRef]